PHYSICOCHEMICAL STUDIES
OF SYSTEMS AND PROCESSES

Development of Yttrium and Iron Oxide Thin Films via AACVD Method for Photooxidation of Water

Raffia bintay Yousaf[a], Shahzad Abu Bakar[b], Muhammad Mazhar[a], Muhammad Adil Mansoor[a], and Mudassir Iqbal[a,*]

[a] Department of Chemistry, School of Natural Sciences, National University of Sciences and Technology, H-12, Islamabad, 44000 Pakistan
[b] Nanosciences and Technology Department, National Center for Physics, Islamabad, 44000 Pakistan
*e-mail: mudassir.iqbal@sns.nust.edu.pk

Abstract—Owing to high stability, metal oxide-based ceramic thin films are of great interest for photocatalytic oxidation of water. Therefore, the current research is focused on the fabrication of different transition metal oxide thin films to estimate their photocatalytic efficiency. In the present research thin films of oxides of iron and yttrium are prepared on FTO glass substrate via Aerosol Assisted Chemical Vapor Deposition (AACVD) from methanol solution of iron and yttrium acetate precursors. The deposition of targeted films Fe_2O_3 and Y_2O_3 were carried out at 420 and 450 °C respectively under the argon gas flow of 120 cm³/min. Thin films were characterized by Fourier transform infrared spectroscopy (FT-IR), X-ray diffraction (XRD), field emission scanning electron microscopy (FESEM), to determine their phase and morphology. The direct energy band gaps were determined *via* Tauc's plot that gave values of 2.05 eV and 3.3 eV for oxides of iron and yttrium respectively. The photoelectrochemical water splitting response of the as-fabricated transition metal oxide as working electrodes were measured using linear scan voltammetry. The maximum value of photocurrent density recorded under the illumination with xenon lamp at 1.2 V vs. RHE was equal to 2.5 mA/cm² and 0.3 mA/cm² for Fe_2O_3 and Y_2O_3 thin films, respectively.

Keywords: iron oxide, yttrium oxide, bandgap, AACVD, photocurrent

DOI: 10.1134/S1070427222010050

INTRODUCTION

The continuous depletion of fossil fuel has emerged the demand for some alternate, environmentally benign source of energy [1-5]. As the demand for energy rises to power industries, the need for the development of alternative energy resources has also increased. Furthermore, global warming and environmental depletion are also related to the continuous emission of greenhouse gases into the natural environment [6–8]. To meet these challenges, the development of environment-friendly, proficient, sustainable, and cost-effective energy sources are employed. Hydrogen (H_2) is efficient fuel that is free of hazardous gasses emission to the environment and can be used in fuel cells to produce electricity [9-11]. Hydrogen can be regarded as an efficient, green, and clean fuel only if it is generated by using the renewable resource of energy [12]. The photoelectrochemical water splitting for hydrogen generation is an ecologically friendly method. This technique of hydrogen generation using solar irradiation as a primary energy source is known as photolysis [1–5, 13]. Remarkable work has been done in the field of photolysis after the first innovation of photoelectrochemical mechanisms by Honda and Fujishima [14]. Initially, the titania was used as a photocatalyst for water splitting, however, due to high bandgap it could only work in UV light, whereas most of the portion of solar light that approached land is of the visible region, Thus, there is a need of such active photocatalyst that can work in the visible region of light [15–17]. The photoelectrochemical (PEC) system for water splitting is based on materials that can absorb in the middle region of light with the preamble band gap of 1.6–2.5 eV. This bandgap is enough to interact and split

water into hydrogen and oxygen [18, 19]. Apart from band gap, band edges also play a vital role in the oxygen evolution reaction of hydrogen production reaction. Several electrodes such as metal oxides, metal sulfides, metal nitrides, metal-organic frameworks have been examined for their photocatalytic conversion of water into hydrogen and oxygen [20–24]. Moreover, the stability of photoelectrodes in different electrolyte environments is also an important aspect for reproducibility and repeatability of material for a long time. In this regard, metal oxide semiconductors have shown good efficiency to act as photoelectrodes due to their wide distribution of the bandgap, low electrical resistance, flat band potential, easily tunable electronic properties, stability, low cost, facile fabrication and show good resistance to corrosion in aqueous solution [25–27].

Solid thin films of metal oxides are developed in the form of a thin layer on a solid support, known as substrate. These are formulated through the condensation of discrete ionic, molecular, or atomic species at or near the surface of the substrate [28]. Thin films have shown better efficiency in photoelectrochemical water splitting due to the distinctive properties of the thickness, geometry, and structure of the film [29–31]. Various factors significantly affect the competence of thin films for water splitting, such as variations in crystalline structure and surface characteristics of the semiconductor photoelectrodes. By changing the deposition condition and method we can alter the above-mentioned properties of thin-film as well as their PEC performance [32]. Aerosol Assisted Chemical Vapor Deposition (AACVD) is particularly interesting, as high temperature or pressure is not necessary to generate the gaseous precursors. It provides numerous benefits over other methods such as being relatively cheaper, providing better stoichiometry control, control over surface morphology, and simpler arrangement [33]. Furthermore, by precisely selecting the deposition conditions (i.e. solvent, deposition temperature) thin films of different morphology are obtained which consequently affect the functional properties of the material [34, 35]. Previously, Fe_2O_3 has been prepared by different techniques such as anodization, sol-gel method, Chemical vapour deposition etc. and has shown different values of photocurrent density such as 0.59, 0.6, 0.75, 1.23, 0.19, and 2.2 mA cm^{-2} at applied potential of 1.2 V against reversible hydrogen electrode [36–41]. While the oxides of yttrium display various fascinating and auspicious physical properties like thermal stability, good chemical durability, high mechanical strength, and thermal conductivity [42]. To the best of our knowledge, pure yttrium oxide is not employed for photoelectrochemical studies. However, several studies show the use of yttrium as a host or dopant with other materials such as CuO, Fe_2O_3, and ZrO_2 for photoelectrochemical properties [43–45]. Therefore, the present study is focused on the fabrication phase pure Y_2O_3 and Fe_2O_3 thin films via AACVD using their respective acetate precursors from a methanol solution. As-synthesized films are then used for their photoelectrochemical properties.

MATERIALS AND METHODS

Materials

All the solvent, reagents, and chemicals *viz.* methanol, trifluoroacetic acid, iron acetate, yttrium acetate were purchased from Sigma Aldrich (China) with 99.9% purity and were used without further purification. All the experimental manipulations for making precursor solutions were carried out under an inert atmosphere of dry argon using Schlenk tubes and vacuum line techniques. FTO glass substrate with a thickness of 2.2 mm, a resistance of 6–8 ohm/sq, and a transmittance of 80–85% were purchased from Sigma Aldrich, China.

Thin Film Fabrication

The thin films were deposited on commercially available FTO-coated glass substrate using a self-designed AACVD assembly as described elsewhere [21]. The FTO-coated glass substrate was purchased from Sigma Aldrich and was cut to the dimension of 25.4 × 2.7 × 2.2 mm (L × W× D) and then cleaned by ultrasonically washing with distilled water, acetone, and then ethyl alcohol. Finally, they were washed with distilled water, stored in ethanol, and dried in the air before use. FTO substrate slides of the dimension of 25.2 mm × 12.7 mm were placed inside a tube furnace chamber and then heated up to the deposition temperature for 10 min before carrying out the deposition. The aerosol of the precursor solution was formed by keeping the round-bottom flask in a water bath above the piezoelectric modulator of an ultrasonic humidifier. The generated aerosol droplets of the precursor were transferred into the hot wall zone of the reactor by the carrier gas. At the end of the deposition, the aerosol line was closed, and a carrier gas stream

was passed over the substrates until the chamber cools down to room temperature before they were removed for studies [11]. In a typical experiment, 0.25 mmol of the precursor was dissolved in 25 mL of methanol to deposit thin films of metal oxide on FTO-conducting glass under Argon gas with a flow rate of 120 cm^3 min^{-1}. The iron oxide and yttrium oxide thin films were deposited at two different temperatures of 420 and 450°C from the iron acetate and yttrium acetate precursors, respectively. The films were uniform, mechanically robust, stable in atmospheric conditions, and well adhered to FTO substrate as verified by the "scotch tape test" [46].

Characterization of Thin Films

FT-IR spectra were recorded on an attenuated total reflectance (ATR) instrument (4000–400 cm^{-1}, resolution 4 cm^{-1}). The surface morphology of thin films was studied using a field-emission gun scanning electron microscope (FESEM, /FEI Quanta 400) coupled with Energy Dispersive X-ray spectrometer EDX INCA Energy 200 (Oxford Inst.) at an accelerating voltage of 20 kV, 20,000 magnifications, and a working distance of 9 mm. The structural characteristic of the as-fabricated films was characterized using X-ray powder diffraction (XRD) on a D8 Advance X-Ray Diffractometer- Bruker AXS using CuK_α radiation (λ = 1.542+/–0.002 Å) at a voltage of 40 kV and current of 40 mA at ambient temperature. The optical absorption spectrum of the thin film was recorded on a Lambda 35 Perkin-Elmer UV-visible spectrophotometer in the wavelength range of 300–800 nm. The photoelectrochemical properties of as-synthesized electrodes were measured using a standard three-electrode electrochemical cell fitted with a quartz window. Ag/AgCl electrode and Pt were employed as the reference and counter electrodes respectively and all the measurements were carried out in 1 M NaOH aqueous electrolyte. Steady-state current-voltage measurements of the films were carried out using a potentiostat (Eco Chemie micro-Autolab type III), while the cells were illuminated by an AM 1.5 Class A solar simulator (Solar Light 16S-300 solar simulator), at 100 mW cm^{-2} light intensity, calibrated by a silicon pyranometer (Solar Light Co., PMA2144 Class II). The effective area of the film was adjusted to 1 × 1 cm^2.

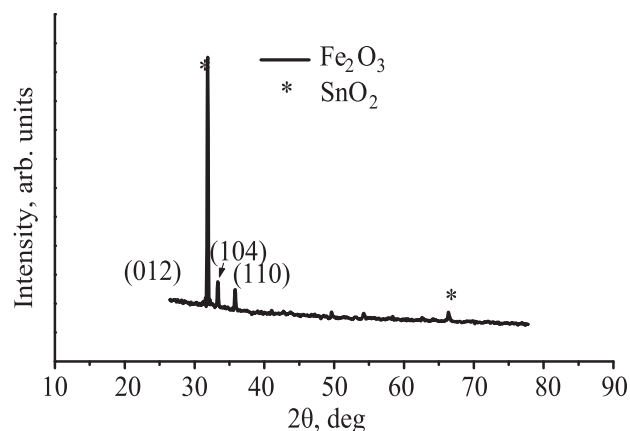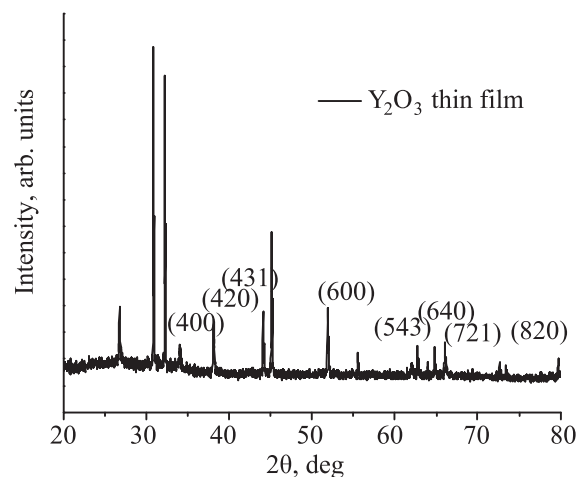**Fig. 1.** XRD peak pattern of as-fabricated of Fe$_2$O$_3$ thin film on FTO substrate using AACVD at 420°C.

Fig. 2. XRD peak pattern of the as-fabricated Y$_2$O$_3$ thin film on the FTO substrate using AACVD at 450°C.

RESULTS AND DISCUSSION

Powder X-ray diffraction

Iron oxide. The crystalline peaks (Fig. 1) at 2θ values of 24.31, 33.32, and 35.79° identify the (012), (104), and (110) rhombohedral crystal of Fe$_2$O$_3$. These values are perfectly matched with the (JCPDS) reference number 00-001-1053 of the hematite (Fe$_2$O$_3$) structure. These Fe$_2$O$_3$ with rhombohedral crystal system retains the R-3c space group. However, the additional lattice reflections at the 2θ position of 31.86 and 66.36 are originated from fluorinated tin oxide-coated glass substrates.

Yttrium oxide. The reflections at 2θ values of 32.2, 38.1, 44.0,52.8, 62.077, 64.2, 66.0 and 79.7 are corresponding to (400), (420), (431), (600), (543), (640), (721) and (820) is of cubic crystalline orientation of yt-
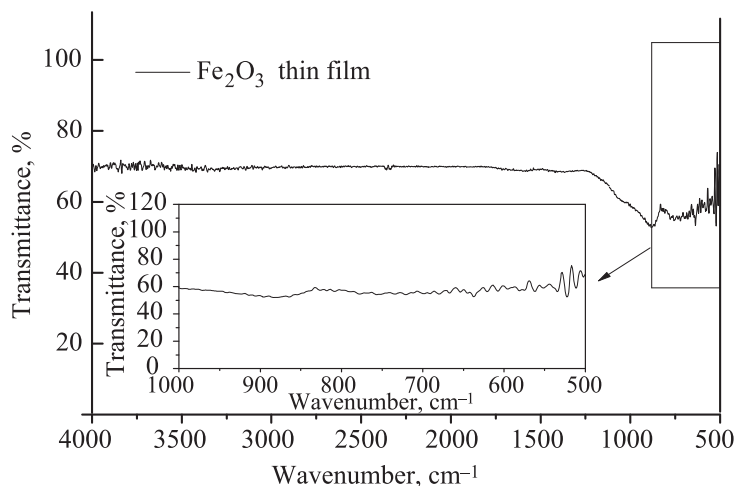
Fig. 3. FTIR spectrum of as-fabricated thin films of Fe_2O_3 upon FTO substrate using AACVD at 420°C.

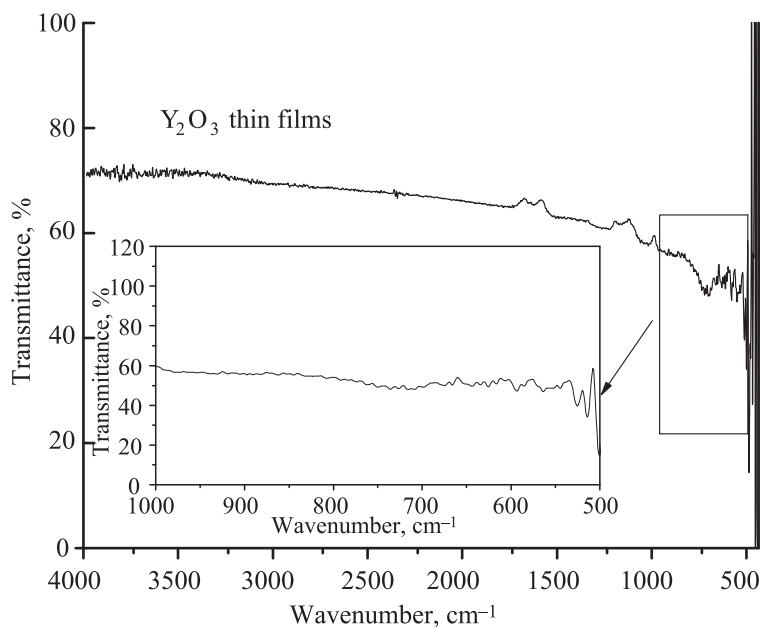**Fig. 4.** FTIR spectrum of as-fabricated Y_2O_3 thin films upon FTO substrate using AACVD at 450°C.

tria (Y_2O_3) films as shown in Fig. 2. These peaks are in good match with JCPDS reference card number 00-041-1105. While the remaining peaks are attributed to tin oxide.

Infrared Spectroscopy

Iron oxide. The vibrational active bands under infrared sources were observed around 520 and 692 cm^{-1} as shown in Fig. 3 and are in good agreement with the literature [47]. This shows the depicting presence of Fe-O vibrations present in the alpha phase hematite Fe_2O_3. However, no significant band was present in the region from 1000 to 4000 cm^{-1} which indicates the absence of

any impurity such as moisture or carbonaceous contamination from the precursor.

Yttrium oxide. The vibrational band around 530 cm^{-1} is associated with the yttrium oxide as per the literature cited value [48]. Similarly, no other peaks for the aforementioned impurities are observed as shown in Fig. 4.

Surface Morphology:

The topographical images of all the synthesized films were studied by scanning electron microscopy (SEM).

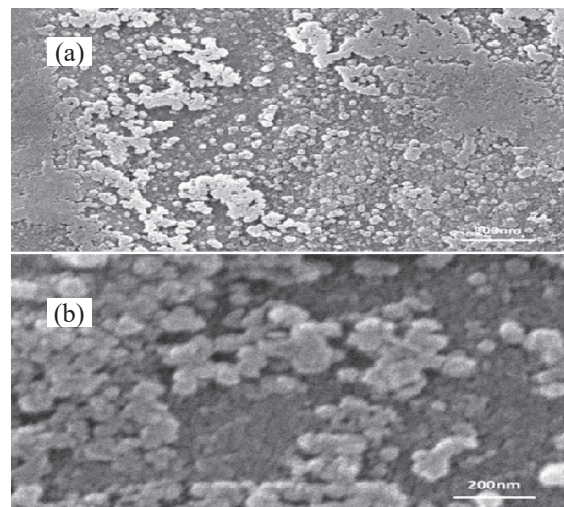**Iron Oxide.** Figure 5 shows the SEM images of as-fabricated Fe_2O_3 thin films on FTO substrate using
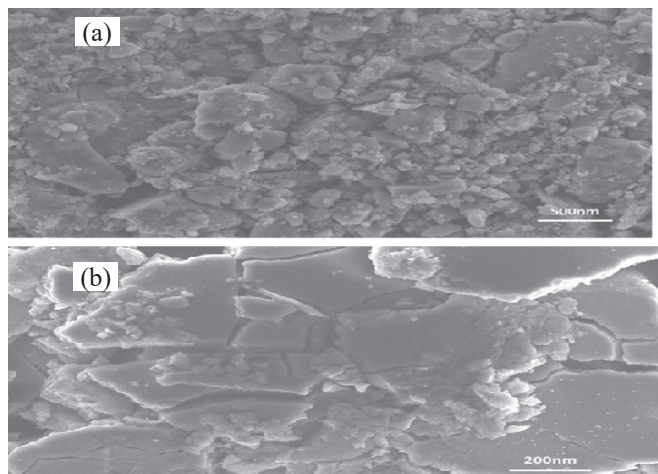
Fig. 5. (a, b) Surface morphological study showing the SEM images of Fe_2O_3 thin films deposited at 420°C.

Fig. 6. (a, b) Surface morphological studies showing the SEM images of the Y_2O_3 thin films at 450°C.

a single-source precursor at 420°C. The SEM images illustrate the formation of irregularly shaped nanoparticles that are well connected and uniformly distributed all over the substrate. The particle size of the grains is in the range of 60–120 nm. Somewhere, particles are seemed to be agglomerated. However, connectivity and porosity are not affected. It is believed that uniform connection of particles facilitates fast transportation of charge carriers i.e. photoinduced charges. This is expected due to the generation of electronic connections among the inter-linked particles during the growth of Fe_2O_3 thin films. The particles at the surface of thin films are uniformly distributed to form a compact surface. The inter-linked particles have a porous structure which resulted in a high internal surface area of the films. It is evident that the presence of such structure enabled the unique chemical and physical properties of the films and are potential features of the films showing higher photoelectrochemical water splitting efficiency.

Yttrium oxide. Figure 6 shows the SEM images of the as-fabricated Y_2O_3 thin films deposited on the FTO substrate using AACVD. The surface of the films consisted of tiny particles with random orientation and are distributed throughout the surface of the films to form a compact and crack-free surface of the films. The estimated particle size is in the range of 80−150 nm. Surface roughness is also prominent that is effective for electrolyte interaction with deeper layers of film

Optical band gap studies. A detailed study has been carried out to analyze the optical properties of the as-

fabricated transition metal oxide thin films using diffuse reflectance spectroscopy. The Kubelka–Munk function F(R); was used to estimate the transition between extended conduction and valence bands states. Relation between reflectance and Kubelka–Munk function is given in the following equation:

$$F(R) = \frac{(1-R)^2}{2R},\qquad(1)$$

where, R and $F(R)$ represents diffuse reflectance of the sample and Kubelka–Munk function, respectively. The bandgap is calculated by the tauc's plot between the square of modified Kubelka–Munk function $F(R)$ against photon energy ($h\upsilon$). Obtained values of bandgap calculated by using the above relation for the synthesized transition metal oxides thin films are discussed in the following section.

Iron oxide. The DRS spectrum of bare FTO was recorded to remove the effect of substrate. The value was calculated by plotting a graph between the square of $F(R)$ and photon energy (Fig. 7). The optical direct bandgap value of Fe_2O_3 was found to be 2.05 eV which is in good match with the reported value [49]. It is believed that this is a good value for water splitting.

Yttrium oxide. Similarly, the bandgap energy of the Y_2O_3 thin films was ~3.3 eV (Fig. 8) which is quite low as compared to the reported value [50]. It is reported that in the case of polycrystalline thin films, the presence of a higher concentration of the charge carrier and the forma-

**Table 1.** A comparative study of present work with literature

| Series no.	Material used	Method of synthesis	Applied potential	Photocurrent density, mA cm^{-2}	Reference.
1	α-Fe$_2$O$_3$	Anodization of Fe foil	1.5 V vs RHE	0.5	51
2	α-Fe$_2$O$_3$/ γ-Fe$_2$O$_3$	Reverse micelle deposition	1.4 V vs RHE	0.8	52
3	α-Fe$_2$O$_3$/Pt	Ultrasonication	2 V vs Ag/AgCl	0.8	53
4	α-Fe$_2$O$_3$	AACVD	1.23 V Vs RHE	0.45	54
5	α-Fe$_2$O$_3$	AACVD	1.2 V vs RHE	2.5	Present work
6	CuYO$_2$–0.5Cu$_2$O	AACVD	1.0 V vs SCE	0.008	55
7	Y$_2$CuO$_4$–5CuO	AACVD	0.8 V vs SCE	0.001	56
8	Y$_2$O3	AACVD	1.2 V vs RHE	0.3	Present work

tion of potential barriers at the boundaries of the crystallite enhanced the bandgap energy value. This means that the thin films have larger crystallite boundaries as compared to the crystallite size. Whereas the presence of disorders and defects/vacancies in the surface of the thin film reduces the bandgap energy value due to the existence of the localized states. Thus, the lower band gap value of the as-fabricated Y$_2$O$_3$ thin films is expected due to the presence of disorder and defects in the thin films.

Photoelectrochemical studies. The photoelectrochemical (PEC) studies were estimated via a standard three-electrode arrangement in which, metal oxide thin film was used as photoactive working electrode, Ag/AgCl/3M KCl as reference electrode, and a Pt counter electrode in 1 M solution of NaOH. The scan rate dur-

ing the PEC measurements was 20 mV/s. The potential applied against Ag/AgCl was converted into concerning standard hydrogen electrode potential via the Nernst equation. It was observed that no significant amount of current was produced at the applied potential of 1.4 V under dark conditions. However, under illumination conditions using Xe lamp (OPS-A500, Newport) of power of 150 mW cm^{-2}, Iron oxide a photocurrent density of 2.5 mA/cm^2 at 1.2 V (Fig. 9) was observed. The onset potential for these films is equal to 0.7 V. This current density response under simulated light is well established that the prepared photoanode had an excellent light response and exceptional stability.

Yttrium oxide. In the case of yttrium oxide films, current response in dark and under light irradiation was
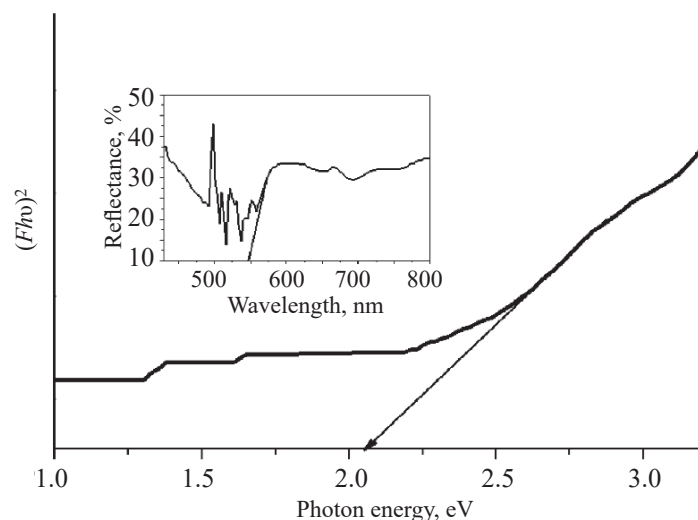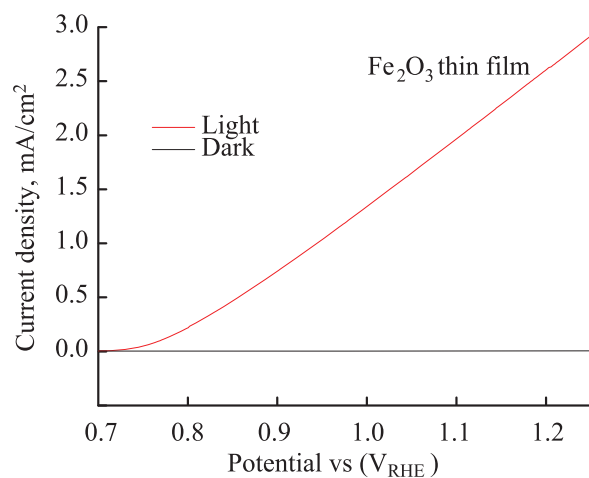

Fig. 7. Bandgap calculations of as-fabricated Fe$_2$O$_3$ thin films upon FTO substrate using AACVD at 420°C inset shows the DRS spectra.
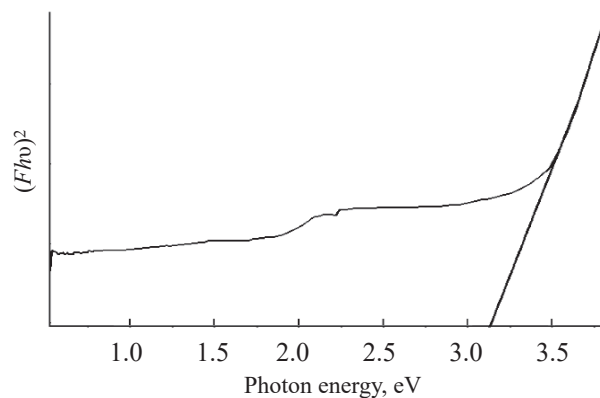
Fig. 8. Bandgap calculations of as fabricated Y_2O_3 thin film upon FTO substrate using AACVD at 450°C inset shows DRS spectra.

calculated by the same procedure. The result obtained in this case is shown in Fig. 10. Y_2O_3 thin films yielded an amount of current which is equal to almost 0.3 mA/cm^2 under an applied potential of 1.2 V while the onset potential of the yttria films is 0.8 V.

In the case of Fe_2O_3, the current density observed is higher as compared to yttrium oxide. These results are further supporting the bandgap values calculated for the fabricated films using DRS as described above. Although the onset potential is almost similar in both films. The photoexcited charge carrier i.e. holes and electrons interact with the ions in the solution to start the redox reaction at their respective electrode with the liberation of gases. This proves that the presence of optimum band gap energy values played an important role in the PEC
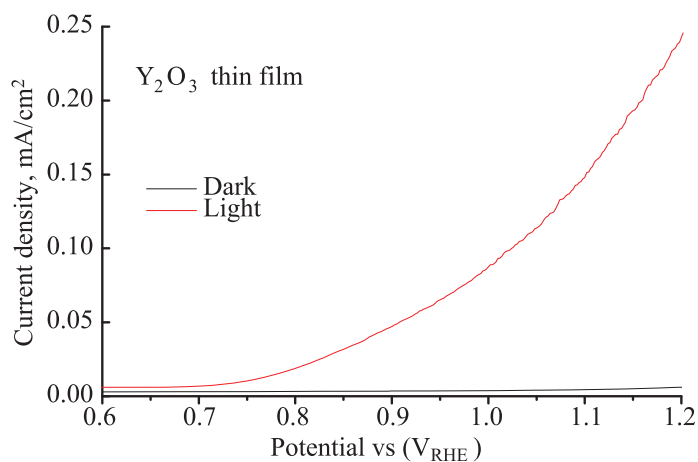
study of the fabricated thin films. Furthermore, a comparative study of present work with literature is summarized below in Table 1.

CONCLUSIONS

A feasible and easy method was employed for the deposition of iron and yttrium oxide thin films using respective metal acetate as a single-source precursor. The as-fabricated thin films were characterized for their structural, optical, and morphological properties using XRD, UV-vis spectroscopy, and FE_SEM analysis. The XRD analysis of the as-fabricated thin films confirmed the formation of stable phases of the corresponding metal oxide. The bandgap energy values of as-fabricated thin films were found to be ~2.05 eV and ~3.3 eV for iron and yttrium oxides, respectively. The as-fabricated thin films were tested as working electrodes for their potential PEC study using linear cyclic voltammetry. It was observed that the as-fabricated iron and yttrium oxide thin films showed reasonable photocurrent density of 2.5 mA/cm^2 and 0.3 mA/cm^2 under an applied potential of 1.2 V which suggests their potential use for energy harvesting applications.

ACKNOWLEDGMENTS

Fig. 9. (Color online) Linear sweep voltammetry curve for as-synthesized iron oxide thin films under dark and illumination conditions

Fig. 10. (Color online) Linear sweep voltammetry curve for as-synthesized yttrium oxide thin films under dark and illumination conditions.

CONFLICTS OF INTEREST

The authors declare no conflicts of interest.

REFERENCES

1. Suga, M., Akita, F., Hirata, K., et al., *Nature*, 2015, vol. 517, no. 7532, pp. 99–103.

2. Tsui, E.Y., Kanady, J.S. and Agapie, T., *Chem.*, 2013, vol. 52, no. 24, pp. 13833–13848.

3. Ismail, A.A. and Bahnemann, D.W., *Sol. Energy Mater. Sol. Cells*, 2014, vol. 128, pp. 85–101.

4. Maeda, K. and Domen, K., *J. Phys. Chem. Lett.*, 2010, vol. 1, no. 18, pp. 2655–2661.

5. Noel, N.K., Stranks, S.D., Abate, A., et al., *Energy Environ. Sci.*, 2014, vol. 7, no. 9, pp. 3061–3068.

6. Ren, X., Zi, W., Ma, Q., et al., *Sol. Energy Mater. Sol. Cells*, 2015, vol. 134, pp. 54–59.

7. Green, M.A., Ho-Baillie, A. and Snaith, H.J., *Nat. Photonics*, 2014, vol. 8, no. 7, pp. 506–514.

8. Mansoor, M.A., Ismail, A., Yahya, R., et al., *Inorg. Chem.*, 2013, vol. 52, no. 10, pp. 5624–5626.

9. Zohuri, B. and McDaniel, P., *Springer International Publishing,* 2019, pp. 23–67

10. Güney, T., *Int. J. Sustain. Dev. World Ecol.*, 2019, vol. 26, 5, pp. 389–397.

11. Panwar, N.L., Kaushik, S.C. and Kothari, S., *Renew. Sustain. Energy Rev.*, 2011, vol. 15, 3, pp. 1513–1524.

12. Hosseini, S.E. and Wahid, M.A., *Renew. Sustain. Energy Rev.*, 2016, vol. 57, pp. 850–866.

13. Mansoor, M.A., Munawar, K., Lim, S.P., et al., *New J. Chem.*, 2017, vol. 41, no. 15, pp. 7322–7330.

14. Fujishima, A. and Honda, K., *Nature*, 1972, vol. 238, no. 5358, pp. 37–38.

15. Dong, Z., Ding, D., Li, T. and Ning, C., *Appl. Surf. Sci.*, 2019, vol. 480, pp. 219–228.

16. Kusior, A., Wnuk, A., Trenczek-Zajac, A., Zakrzewska, K. and Radecka, M., *Int. J. Hydrogen Energy*, 2015, vol. 40, no. 14, pp. 4936–4944.

17. Tan, C. and Zhi, Q., *The Energy-Water Nexus,* 2016, vol. 88, pp. 277–284.

18. Jian, J., Jiang, G., van de Krol, R., Wei, B. and Wang, H., *Nano Energy*, 2018, vol. 51, pp. 457–480.

19. Mansoor, M.A., Huang, N.M., McKee, V., et al., *Sol. Energy Mater. Sol. Cells*, 2015, vol. 137, pp. 258–264.

20. Mansoor, M.A., Mazhar, M., Ebadi, M., Ming, H.N., Mat Teridi, M.A. and Kong Mun, L., *New J. Chem.*, 2016, vol. 40, no. 6, pp. 5177–5184.

21. Chen, Z., Duan, X., Wei, W., Wang, S. and Ni, B.-J., *J. Mater. Chem. A*, 2019, vol. 7, no. 25, pp. 14971–15005.

22. Yu, F., Zhou, H., Zhu, Z., et al., *ACS Catal.*, 2017, vol. 7, no. 3, pp. 2052–2057.

23. Wang, W., Dong, J., Ye, X., Li, Y., Ma, Y. and Qi, L., *Small*, 2016, vol. 12, no. 11, pp. 1469–1478.

24. Khan, I., Ali, S., Mansha, M. and Qurashi, A., *Ultrason. Sonochem.*, 2017, vol. 36, pp. 386–392.

25. Pankratov, D.A., Veligzhanin, A.A. and Zubavichus, Y.V., *Russ. J. Inorg. Chem.*, 2013, vol. 58, no. 1, pp. 67–73.

26. D'yachkov, E.P. and D'yachkov, P.N., *Russ. J. Inorg. Chem.*, 2019, vol. 64, no. 9, pp. 1152–1155.

27. D'yachkov, E.P. and D'yachkov, P.N., *Russ. J. Inorg. Chem.*, 2018, vol. 63, no. 9, pp. 1204–1210.

28. Hardwick, D.A., *Thin Solid Films*, 1987, vol. 154, no. 1–2, pp. 109–124.

29. Wilson, N.C., Muscat, J., Mkhonto, D., Ngoepe, P.E. and Harrison, N.M., *Phys. Rev. B*, 2005, vol. 71, no. 7, p. 075202.

30. Nozik, A.J., *Phys. Rev. B*, 1972, vol. 6, no. 2, pp. 453–459.

31. Zhang, T., Shen, Y. and Zhang, R., *Mater. Lett.*, 1995, vol. 23, no. 1–3, pp. 69–71.

32. Mansoor, M.A., Ebadi, M., Mazhar, M., et al., *Mater. Chem. Phys.*, 2017, vol. 186, pp. 286–294.

33. Tahir, A.A., Ehsan, M.A., Mazhar, M., Wijayantha, K.G.U., Zeller, M. and Hunter, A.D., *Chem. Mater.*, 2010, vol. 22, no. 17, pp. 5084–5092.

34. Munawar, K., Mansoor, M.A., Olmstead, M.M., et al., *Mater. Chem. Phys.*, 2020, vol. 255, p. 123220.

35. Zan, R. and Altuntepe, A., *J. Mol. Struct.*, 2020, vol. 1199, p. 127026.

36. Emin, S., de Respinis, M., Mavrič, T., Dam, B., Valant, M. and Smith, W.A., *Appl. Catal. A Gen.*, 2016, vol. 523, pp. 130–138.

37. Jia, L., Harbauer, K., Bogdanoff, P., et al., *J. Mater. Chem. A*, 2014, vol. 2, no. 47, pp. 20196–20202.

38. Bosso, P., Milella, A., Barucca, G., et al., *Plasma Process. Polym.*, 2021, vol. 18, no. 1, p. 2000121.

39. Wickman, B., Bastos Fanta, A., Burrows, A., Hellman, A., Wagner, J.B. and Iandolo, B., *Sci. Rep.*, 2017, vol. 7, no. 1, p. 40500.

40. Kay, A., Cesar, I. and Grätzel, M., *J. Am. Chem. Soc.*, 2006, vol. 128, no. 49, pp. 15714–15721.

41. Kyesmen, P.I., Nombona, N. and Diale, M., *Mater. Res.*

Bull., 2020, vol. 131, p. 110964.

42. Gaboriaud, R.J., Pailloux, F., Guerin, P. and Paumier, F., *J. Phys. D. Appl. Phys.*, 2000, vol. 33, no. 22, pp. 2884–2889.

43. Reddy, I.N., Reddy, C.V., Cho, M., Kim, D. and Shim, J., *J. Electroanal. Chem.*, 2019, vol. 848, p. 113335.

44. Reddy, C.V., Reddy, I.N., Shim, J., Kim, D. and Yoo, K., *Ceram. Int.*, 2018, vol. 44, no. 11, pp. 12329–12339.

45. Käämbre, T., Vanags, M., Pärna, R., et al., *Ceram. Int.*, 2018, vol. 44, no. 11, pp. 13218–13225.

46. Larsen, P.K., Cuppens, R. and Spierings, G.A.C.M., *Ferroelectrics*, 1992, vol. 128, no. 1, pp. 265–292.

47. ATR-FT-IR spectra of Iron(III) oxide (Fe₂O₃). http://lisa.chem.ut.ee/IR_spectra/paint/fillers/ironiii-oxide/

48. Alarcón-Flores, G., Aguilar-Frutis, M., García-Hipolito, M., Guzmán-Mendoza, J., Canseco, M.A., and Falcony, C., *J. Mater. Sci.*, 2008, vol. 43, no. 10, pp. 3582–3588.

49. Lassoued, A., Dkhil, B., Gadri, A., and Ammar, S., *Results Phys.*, 2017, vol. 7, pp. 3007–3015.

50. Ivanic, R., Rehacek, V., Novotny, I., et al., *Vacuum*, 2001, vol. 61, no. 2–4, pp. 229–234.

51. Makimizu, Y., Nguyen, N.T., Tucek, J., et al., *Chem Euro J.*, 2019 Vol. 26, pp. 2685 –2692

52. Tokubuchi, T., Arbi, R.I., Zhenhua, P., Katayama, K., et al., *J. Photochem. Photobiol. A: Chem.*, 2021, vol. 410, p. 113179

53. Li, X., Wang, Z., Zhang, Z., et al., *Sci Rep*, 2015, vol. 5, p. 9130.

54. Tahir, A.A., Mat-Teridi, M.A., and Wijayantha, K.G.U., *Rapid Res. Lett.*, 2014, vol. 8, no. 12, pp. 976–981.

55. Ahmed, S., Mansoor, M.A., Basirun,W.J., et al., *New J. Chem.*, 2015, vol. 39, pp. 1031–1037.

56. Ahmed, S., Mansoor, M.A., Mazhar, M., et al., *Dalton Trans.*, 2014, vol. 43, pp. 8523–8529.